Chem Catalysis

CellPress

Article

Ga doping disrupts C-C coupling and promotes methane electroproduction on CuAl catalysts

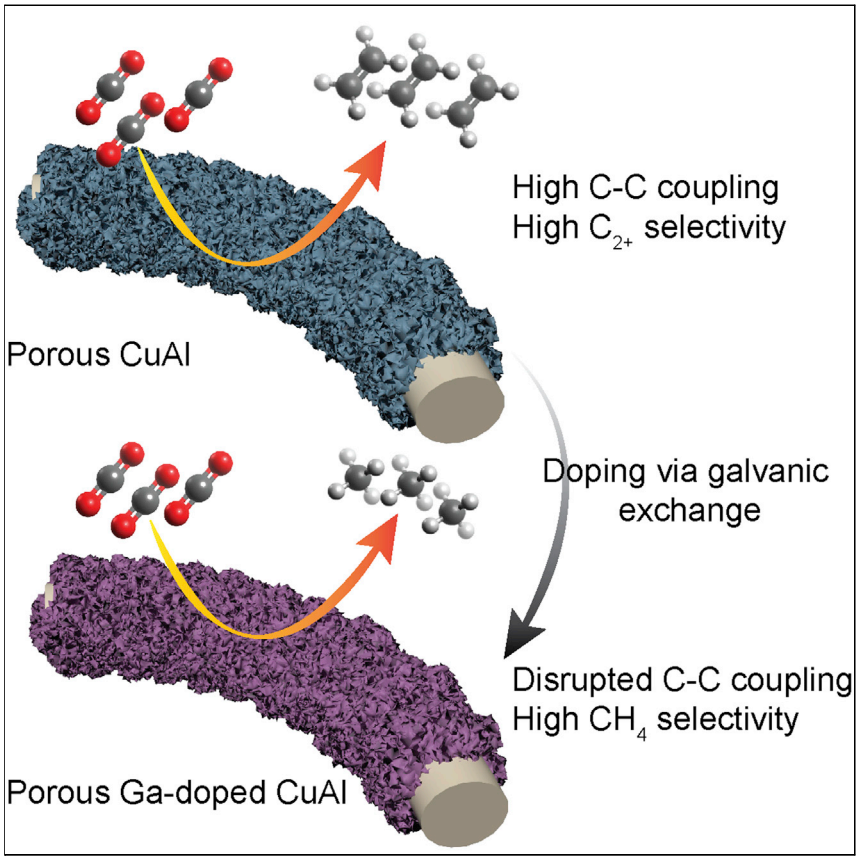

We shift the CO_2 reduction reaction (CO_2RR) product distribution from C_{2+} products toward methane. Ga doping in CuAl catalysts disrupts carbon-carbon coupling and results in a selectivity shift from ethylene to methane while maintaining low hydrogen evolution activity.

Armin Sedighian Rasouli, Xue Wang, Joshua Wicks, ..., Koen Bertens, Jianan Erick Huang, Edward H. Sargent

ted.sargent@utoronto.ca

Highlights

Tuning the CO_2 reduction reaction product distribution by disrupting C-C coupling

Porous Ga-doped CuAl catalysts were synthesized

Methane current density of 234 mA/cm^2 and faradaic efficiency of 53% were achieved

Stable operation over 10 h

Sedighian Rasouli et al., Chem Catalysis *2*, 1–9
April 21, 2022
https://doi.org/10.1016/j.checat.2022.03.016

Please cite this article in press as: Sedighian Rasouli et al., Ga doping disrupts C-C coupling and promotes methane electroproduction on CuAl catalysts, Chem Catalysis (2022), https://doi.org/10.1016/j.checat.2022.03.016

Chem Catalysis

CellPress

Article

Ga doping disrupts C-C coupling and promotes methane electroproduction on CuAl catalysts

Armin Sedighian Rasouli,[1] Xue Wang,[1] Joshua Wicks,[1] Cao-Thang Dinh,[1] Jehad Abed,[1] Feng-Yi Wu,[2] Sung-Fu Hung,[1,2] Koen Bertens,[1] Jianan Erick Huang,[1] and Edward H. Sargent[1,3,*]

SUMMARY

The electrochemical CO_2 reduction reaction (CO_2RR) provides a route to store intermittent electricity in the form of fuels like methane. We reasoned that disrupting C-C coupling while maintaining high *CO coverage could enhance methane selectivity and suppress the hydrogen evolution reaction (HER). We studied the effect of doping CuAl, a material at the top of the CO_2RR activity and selectivity volcano plot, with elements having low *CO binding energies: Au, Zn, and Ga. Encouraged by initial improvements in selectivity to methane, we optimized the Ga content and showed that the presence of uniformly dispersed Ga is crucial in CO_2RR-to-methane performance enhancement. We rule out porosity and roughness and conclude that the presence of Ga in the doped catalysts enables high methane selectivity. The Ga-doped CuAl catalysts achieve a methane Faradaic efficiency (FE) of 53% by suppressing HER to 23% in neutral electrolyte at −1.4 V versus reversible hydrogen electrode.

INTRODUCTION

Toward the goal of storing intermittent, seasonably variable, renewable electricity, it is of potential interest to explore and advance the electrochemical production of methane, a commodity for which the infrastructure for transportation, storage, and use is well developed.[1,2]

Previous works used different strategies to boost the methane selectivity, such as $Cu^{(I)}$-based catalysts,[3] doping Cu structures with metal oxides clusters,[4,5] tuning the CO_2 partial pressure,[6,7] low-coordination-number Cu clusters,[8] and metal-free C-based catalysts.[9] However, Cu alloying and doping elements into Cu-based structure have yet to contribute to selective CO_2RR-to-methane performance of Cu at industrially relevant production rates. Cu is selective toward hydrocarbons,[10,11] and doping different elements—particularly d-block, group 3A, and 4A elements[6,12–18]—into Cu offers avenues to improve CO_2RR selectivity toward a specific product via tuning the reaction intermediate binding energies, and thus, product distributions are affected by the chemical composition and available binding sites of the catalyst.[19] Synthesis methods to achieve these doped Cu materials, such as co-sputtering,[13,20] co-electrodeposition,[12] and galvanic exchange,[18,21] result in different product distributions.

In the present work, we sought a Cu-based methane-selective catalyst to simultaneously suppress the hydrogen evolution reaction (HER) and C_{2+} production. Prior works have indicated a trade-off in electrocatalyst design for methane: lowering the CO_2 partial pressure leads to lower *CO coverage and suppresses C-C coupling,[6,7] thus benefiting C_1 production, mainly methane, but at the expense of

The bigger picture

The energy grid needs to shift from fossil fuels to renewable energies, such as wind, solar, nuclear, and hydroelectric energy, in order for society to keep below the 1.5°C global warming threshold. One challenge in achieving this goal is the intermittency of wind and solar electricity. An approach is the electrically powered production of methane, a commodity for which the infrastructure for storage, transportation, and use is well developed. CO_2RR-to-methane catalysts are in need of improved selectivity, productivity, and stability. Herein, we show how the CO_2RR product distribution can be redirected from C_{2+} products to methane by disrupting carbon-carbon coupling. The material design principles herein contribute to the roadmap for CO_2RR electrocatalyst design.

Please cite this article in press as: Sedighian Rasouli et al., Ga doping disrupts C-C coupling and promotes methane electroproduction on CuAl catalysts, Chem Catalysis (2022), https://doi.org/10.1016/j.checat.2022.03.016

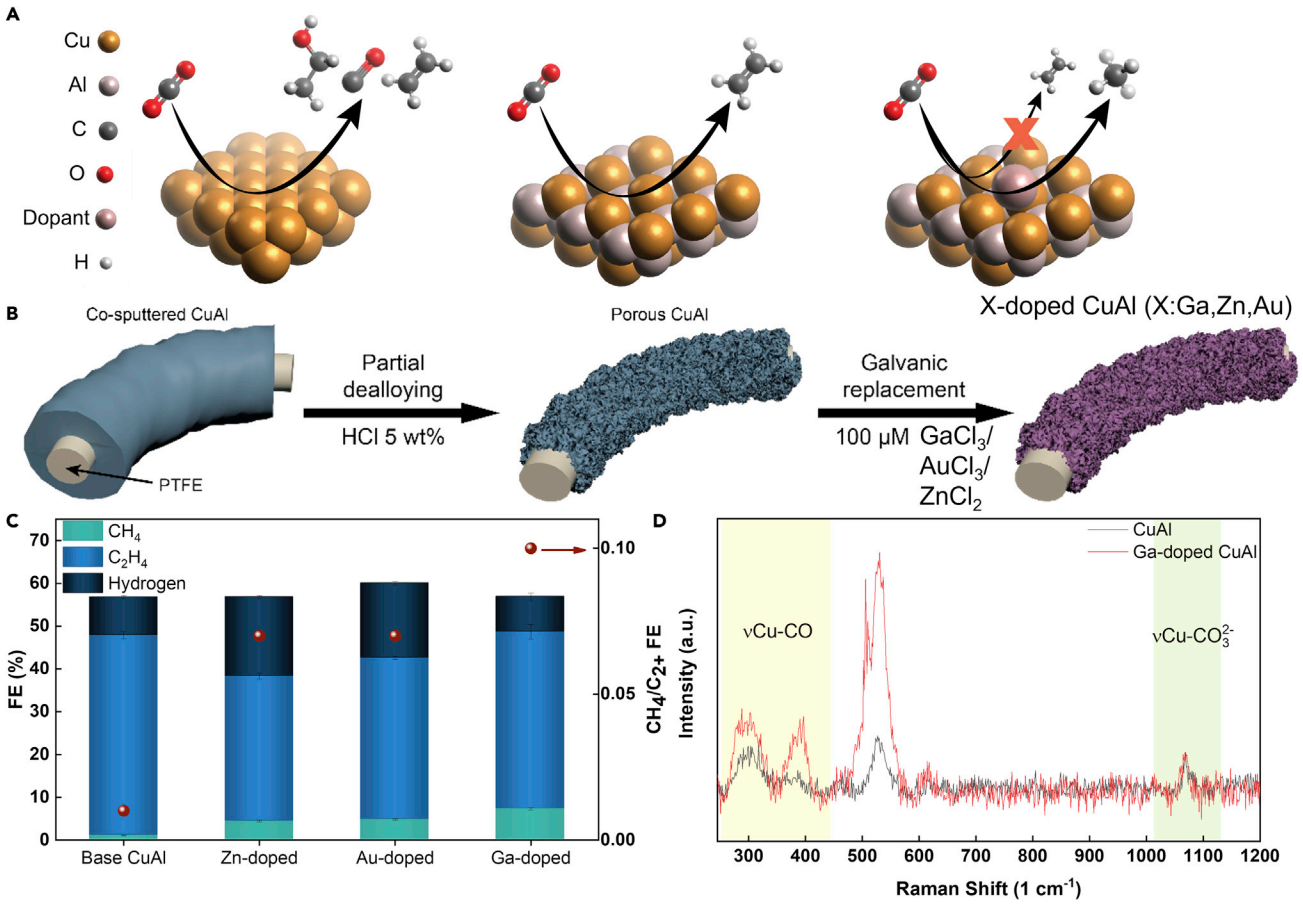

Figure 1. Proposed mechanism and material design principle for C-C disruption

(A) Dopant addition blocks C-C coupling and shifts the product distribution toward methane.

(B) Three-step synthesis method of doped CuAl catalysts.

(C) Gas product FE of CuAl and doped CuAl catalysts with different dopants in 1 M KOH at −1.5 V versus RHE (n = 3 replicates).

(D) Comparison of *in situ* Raman spectra of 8-min Ga-doped CuAl and CuAl catalyst in 1 M $KHCO_3$ with a current density of 25 mA cm^{-2} (−0.9 V versus RHE). The region of 280–430 cm^{-1} showing Cu-CO stretch is shaded.

high HER. Local pH on the catalyst surface affects the CO_2RR product distribution since *CO protonation is a pH-dependent step.[22–25] C-C coupling is disrupted at lower pH, leading to higher selectivity toward methane; however, HER also increases in lower pH.

We pursued therefore a strategy to disrupt C-C coupling in the regime of high *CO coverage since the high *CO coverage can be levered to suppress HER (Figure 1A).[26,27]

We began from a starting point of CuAl binary catalysts since these feature near-ideal *CO binding energies.[20] We posited that adding an element with low *CO binding energies to CuAl catalysts could disrupt C-C coupling.[28,29] We doped base CuAl with Zn, Au, and Ga, which have low *CO binding energies,[29–32] and observed a product distribution shift from C_{2+} products to methane in each case. We optimized Ga-doped CuAl catalysts and reached 53% FE to methane. We studied the optimized Ga-doped CuAl catalysts, which are both porous and rough, and found the improvement in underlying methane activity is from the Ga doping and not due to change in porosity and roughness. *Operando* Raman spectroscopy

[1]Department of Electrical and Computer Engineering, University of Toronto, 35 St. George Street, Toronto, ON M5S 1A4, Canada

[2]Department of Applied Chemistry, National Yang Ming Chiao Tung University, 1001 University Road, Hsinchu 300, Taiwan

[3]Lead contact

*Correspondence: ted.sargent@utoronto.ca

https://doi.org/10.1016/j.checat.2022.03.016

revealed that the introduction of Ga into CuAl tends to increase *CO coverage, resulting in a lower HER. The shift in the product distribution from C_{2+} to methane on Ga-doped CuAl catalysts while maintaining a high *CO coverage indicates that the desired *CO protonation step is promoted compared with the C-C coupling step. We studied Ga-doped CuAl catalysts under −1.4 V versus reversible hydrogen electrode (RHE) and found that these maintained an FE above 45% for over 10 h.

RESULTS AND DISCUSSION

To explore the CO_2RR performance of X-doped (X: Au, Zn, or Ga) CuAl, we synthesized porous catalysts via a three-step method (Figure 1B). Cu and Al are first co-sputtered onto a polytetrafluoroethylene (PTFE) gas diffusion layer (GDL) with a thickness of 200 nm (Figure S1), resulting in a layered hydrophilic/hydrophobic structure—an approach known to enhance the transport of gaseous species.[22] The CuAl layer is then partially dealloyed in 5 wt % HCl solution for T min (4–8 min). Finally, X is added by immersing the CuAl in X chloride solution, leading to the galvanic replacement of Al in the porous CuAl with X. When we attempted extended dealloying exceeding 8 min following galvanic exchange for more than 2 h, we found delamination of the catalyst layer from the PTFE GDL, which we attribute to accelerated corrosion (Figure S2).

We carried out CO_2RR in a flow cell reactor using an alkaline electrolyte (1 M KOH). Compared with CuAl, the series of X-doped 6-min CuAl catalysts (dealloyed for 6 min and doped via galvanic exchange process for 2 h) showed higher methane FE and methane/C_{2+} FE ratio (Figure 1C). We chose Ga-doped CuAl catalysts to investigate the reason behind the methane selectivity increase compared with CuAl through *operando* Raman (Figure 1D).[33] The similar Cu-CO_3^{2-} stretch intensities in base CuAl and Ga-doped CuAl Raman spectra (1,040–1,100 cm^{-1}) indicate a similar surface-enhanced Raman spectroscopy (SERS) effect in Ga-doped CuAl and CuAl. Although Ga-doped CuAl shows higher methane selectivity than CuAl, we found a higher *CO coverage (280–430 cm^{-1}) on the Ga-doped CuAl surface than CuAl. The higher *CO coverage on Ga-doped CuAl may be attributed to *CO intermediate formation on Ga and then the transfer of that to CuAl surface.[17,34] However, we observed a high methane selectivity under high *CO coverage, leading to HER suppression, indicating that Ga addition into CuAl tends to disrupt C-C coupling and facilitate *CO protonation instead. Previous studies have shown the C_{2+} product selectivity generally increases with increasing *CO coverage;[7,35,36] however, at very high *CO coverages, the reaction barrier, enthalpy change of *CO dimerization,[35] and *H binding energies all increase,[37] steering the selectivity away from HER and C_{2+} products. The uniform distribution of Ga increases under-coordinated Cu (Figure S3), leading to stronger *CO binding energies on the Cu surface and preventing its further movement for C-C coupling.[8,34]

We also note that the Ga distribution is more uniform (viz. energy-dispersive X-ray spectroscopy [EDX] mapping; Figures 2A, S4, and S5) in Ga-doped CuAl catalysts compared with Zn and Au distribution in Zn-doped and Au-doped CuAl catalysts. Galvanic replacement occurs between Ga^{3+} and $Al^{(0)}$ on the CuAl surface, since Ga has a standard reduction potential (−0.53 V versus standard hydrogen electrode [SHE]) between Al (−1.66 V versus SHE) and Cu (0.34 V versus SHE).[38] Previous studies on doping Cu-based materials via galvanic exchange have shown that the doping penetration depth is typically limited to 50–100 nm, which is directly correlated with the galvanic exchange kinetics.[39–41] The differences between the standard reduction potentials of the dopants versus Al are higher in the cases of Zn-doped and Au-doped CuAl catalysts compared with that in Ga-doped CuAl

Please cite this article in press as: Sedighian Rasouli et al., Ga doping disrupts C-C coupling and promotes methane electroproduction on CuAl catalysts, Chem Catalysis (2022), https://doi.org/10.1016/j.checat.2022.03.016

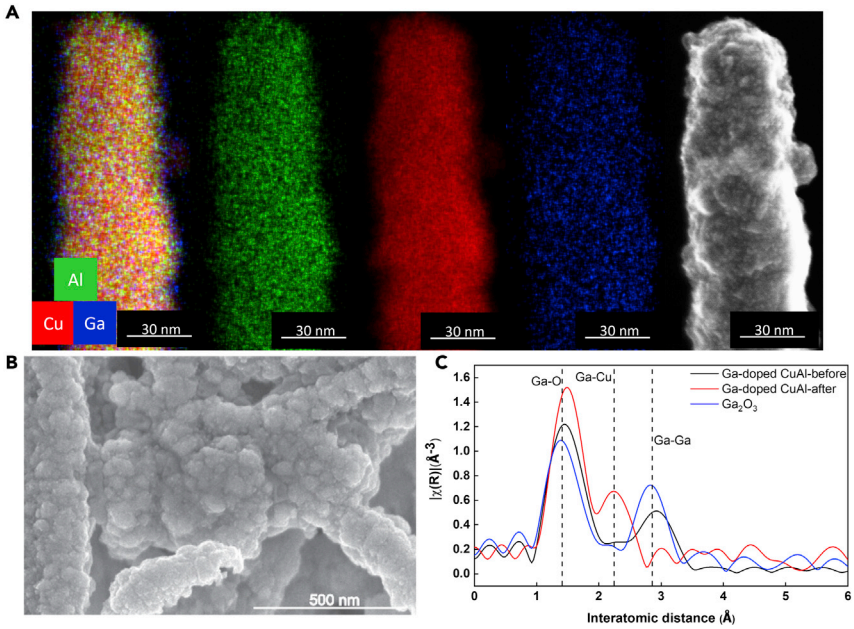

Figure 2. Characterization of Ga-doped CuAl catalysts

(A) EDX mapping and a high-angle annular dark-field scanning transmission electron microscopy (HAADF-STEM) image of Ga-doped 8-min CuAl catalyst.

(B) Scanning electron microscopy image of a representative Ga-doped 8-min CuAl catalyst.

(C) Ga K-edge extended X-ray absorption fine structure (EXAFS) for Ga-doped 8-min CuAl catalyst before and after CO_2RR and reference Ga_2O_3.

catalysts. This accounts for a less uniform distribution of Au and Zn on the CuAl surface than Ga distribution on the CuAl surface (Figure S5).[38,39] We observed high porosity for all the doped CuAl catalysts (Figures 2B and S5). We attribute the low methane selectivity of Au-doped CuAl compared with previously reported CuAu to the difference in inlet CO_2 partial pressure and a non-uniform distribution of Au on CuAl translating into Au agglomeration and large Au-particle formation on the CuAl surface (Figure S5).[6] Higher *H binding energies on the isolated Au surface on Au-doped CuAl compared with Zn- and Ga-doped CuAl surfaces account for increased HER on Au-doped CuAl.[6,42]

To investigate the structure of Ga-doped CuAl under CO_2RR, we performed *ex situ* Ga K-edge X-ray absorption spectroscopy (XAS) and X-ray diffraction (XRD) (Figures 2C, S6, and S7). Before CO_2RR, Ga is present as an oxide (Ga_2O_3), whereas, following CO_2RR, the Ga-Cu peak intensity increases and the Ga-Ga peak decreases. We conclude that the interaction between Cu and Ga increases after CO_2RR, consistent with Ga being dispersed more uniformly (Figure 2C). *Ex situ* Ga K-edge X-ray absorption near-edge structure (XANES) reveals that the white line height increases after CO_2RR (Figure S6): this we attributed to the hybridization of Ga 4p orbitals with those in Cu, increasing empty 4p orbitals, consistent with the view that Ga diffuses in the CuAl structure and forms CuGa alloys. Taking together knowledge of the local pH during CO_2RR, the Ga Pourbaix diagram, and XAS results, we conclude that Ga is in the Ga_2O_3 state before reaction and is part of a Ga-Cu alloy in electroreduction (Figures S7 and S8).

We further optimized the Ga-doped CuAl structure by tuning Ga concentration systematically and studying CO_2RR performance in an alkaline electrolyte (1 M KOH; Figures 3

Please cite this article in press as: Sedighian Rasouli et al., Ga doping disrupts C-C coupling and promotes methane electroproduction on CuAl catalysts, Chem Catalysis (2022), https://doi.org/10.1016/j.checat.2022.03.016

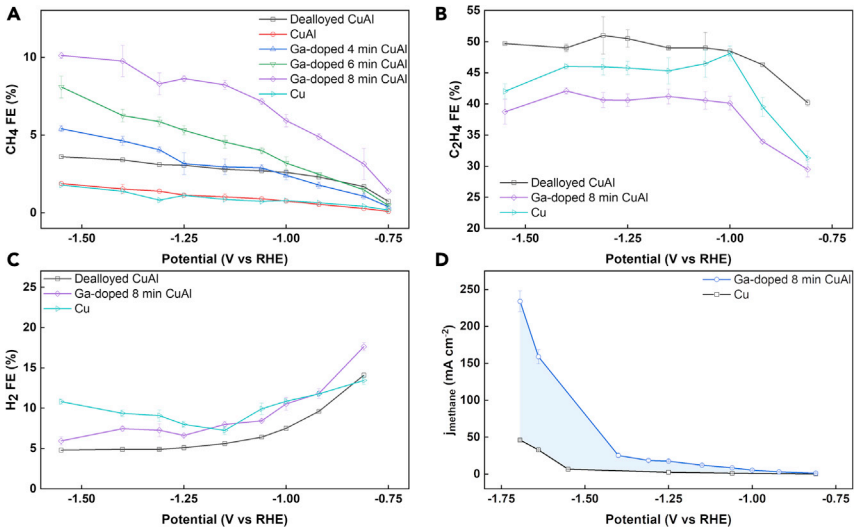

Figure 3. Product distribution of Cu, CuAl, and Ga-doped CuAl catalysts with 1 M KOH electrolyte

(A–C) Methane FE versus potential (A), ethylene FE versus potential (B), and hydrogen FE versus potential (C).

(D) Methane partial current density versus potential (n = 3 independent replicates).

and S9). Methane selectivity increases with dealloying duration (Figure S10). Ga-doped catalysts with Ga concentrations higher than 7.2 wt % show a decrease in both methane and ethylene selectivity: indeed, too much Ga may interfere with Cu active sites. Prior reports reveal that overly high Ga concentration permits the desorption of *CO and may prevent the *CO protonation step needed in methane formation (Figures 2A and S10A), also in agreement with Cu-based binary catalyst studies in which the dopant has a low CO binding energy.[6,13] A computational study predicted that *CO binding energies decrease on CuGa intermetallic catalysts with increasing Ga concentration.[30]

We propose that the addition of Ga to CuAl shifts the product distribution from C_{2+} products to methane by disrupting C-C coupling. We sought to verify the hypothesis, testing the effect of catalyst layer roughness and porosity on performance (Figures S11 and S12; Table S1). We performed CO_2RR experiments on porous Cu: methane FE decreased with increasing porosity, as seen in previous reports.[20] In contrast, the FE on Ga-doped CuAl samples increased with dealloying time, and the roughness of the Ga-doped CuAl samples are very similar, thus linking the increase in methane FE to the addition of Ga, despite the increased surface roughness and porosity that accompanies it.

We found that Ga-doped CuAl catalysts show lower ethylene and C_{2+} product FEs than Cu and dealloyed CuAl catalysts (Figure 3B; Table S2). We observed a lower hydrogen FE on Ga-doped CuAl and dealloyed CuAl than Cu (Figure 3C), hinting at a higher *CO coverage on them that suppresses HER. Ga-doped CuAl catalysts show a higher methane partial current density than Cu, i.e., higher activity (Figure 3D). We obtained a high methane partial current density of 234 mA cm^{-2} at −1.7 V versus RHE with a methane FE of 30% in an alkaline electrolyte with the Ga-doped 8-min CuAl (referred to as Ga-doped CuAl from here onward; Figures 3D and S9D).

To improve further the system-level CO_2RR-to-methane performance, we changed to a neutral pH electrolyte, seeking lower CO_2 crossover[43,44] and also increased

Please cite this article in press as: Sedighian Rasouli et al., Ga doping disrupts C-C coupling and promotes methane electroproduction on CuAl catalysts, Chem Catalysis (2022), https://doi.org/10.1016/j.checat.2022.03.016

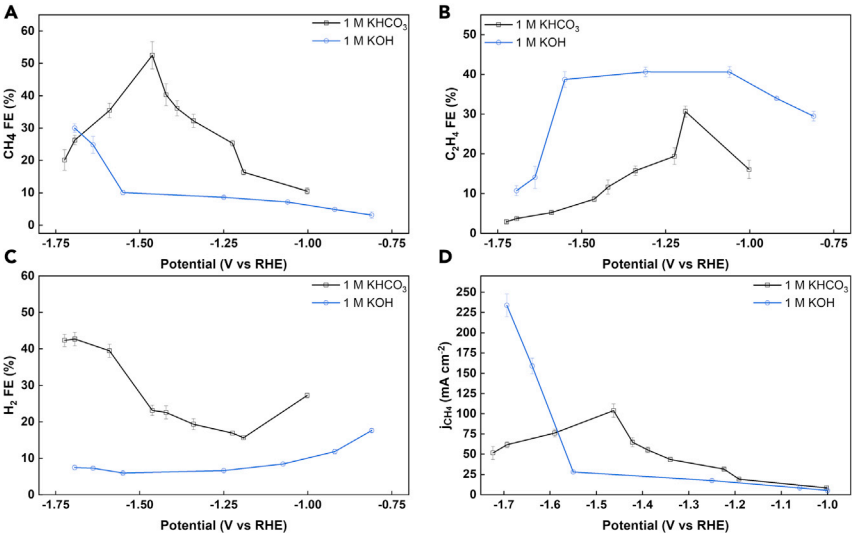

Figure 4. Ga-doped 8-min CuAl CO_2RR performance in a neutral electrolyte (1 M $KHCO_3$) compared with alkaline electrolyte (1 M KOH)

(A–C) Methane FE versus potential (A), ethylene FE versus potential (B), and hydrogen FE versus potential (C).

(D) Methane partial current density comparison between neutral electrolyte (1 M $KHCO_3$) and alkaline electrolyte (1 M KOH) on Ga-doped 8-min CuAl catalysts under different applied potentials (n = 3 independent replicates).

*CO protonation.[45] In 1 M $KHCO_3$ electrolyte, we obtained a methane FE of 53% at −1.4 V versus RHE with a methane partial current density of 109 mA cm^{-2}, accompanied by decreased ethylene FE (Figure 4B). Previous studies have shown that Ga is a CO_2RR-to-CO catalyst, consistent with a low *CO binding energy:[28,29] one possibility is that *CO coverage on non-Ga sites may increase due to the spillover of *CO from Ga to the non-Ga active sites, a phenomenon observed in other Cu-based catalysts containing CO-selective metals.[17,36] We observed a higher methane partial current density in neutral pH electrolyte (1 M $KHCO_3$) with potentials more positive than −1.4 V versus RHE compared with that in an alkaline electrolyte (Figure 4D).

We studied the Ga-doped CuAl catalyst structure following 11 h of operation under CO_2RR at constant potential −1.4 V versus RHE in 1 M $KHCO_3$ (Figure 5). Catalysts showed stable CO_2-to-methane electrolysis for over 10 h, maintaining methane FE above 45% (Figure 5A). We observed no change in the bulk electrolyte pH showing no CO_2 and OH^- loss in the electrolyte, unlike alkaline electrolytes.[46] We characterized the morphology and chemical composition of the catalyst before and after CO_2RR (Figures 5B and 5C). Scanning electron microscopy (SEM) images showed no appreciable changes to surface morphology.

In sum, this work reports Cu-based ternary catalyst materials (doped CuAl) for methane production via CO_2RR. We explored synthesis parameters and achieved a methane FE of 30% in an alkaline electrolyte (1 M KOH) with Ga-doped CuAl catalysts. We further improved the methane FE of Ga-doped CuAl by moving to a neutral electrolyte (1 M $KHCO_3$) and obtained a methane FE of 53% at a methane partial current density of 109 mA cm^{-2} and −1.4 V versus RHE (Table S3). We studied the origins of improved performance in Ga-doped CuAl with *operando* Raman spectroscopy, as well as roughness and porosity control studies. The findings support the

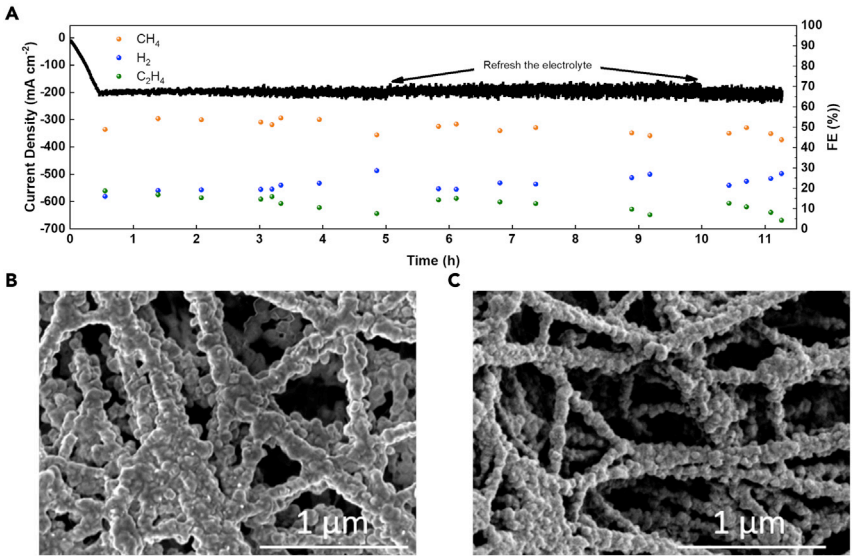

Figure 5. Stability measurements and pre- and post-operation characterization
(A) Ga-doped 8-min CuAl catalyst product distribution under CO_2RR with 1 M $KHCO_3$ as the electrolyte and a constant potential of −1.4 V versus RHE over time (the applied potential was gradually decreased to −1.4 V versus RHE over the first 30 min).
(B and C) SEM images before (B) and after (C) the long-term stability test. The post-CO_2RR characterizations were done on Ga-doped 8-min CuAl after performing CO_2RR for 10 h under −1.4 V versus RHE in 1 M $KHCO_3$.

view that C-C coupling is disrupted by Ga, leading to a product distribution shift from C_{2+} products, including ethylene to methane. We assessed the stability of the Ga-doped CuAl catalyst and observed that the catalyst structure is unchanged during CO_2RR.

EXPERIMENTAL PROCEDURES

An extensive description of materials, sample fabrication, and characterization can be found in supplemental information.

Resource availability

Lead contact

Further information and requests for resources should be directed to and will be fulfilled by the lead contact, Edward H. Sargent (ted.sargent@utoronto.ca).

Materials availability

This study did not generate new unique reagents. Any materials used are available from the lead contact.

Data and code availability

Data are available upon request from the lead contact. No code was generated. Full experimental procedures are provided in the supplemental information.

SUPPLEMENTAL INFORMATION

Supplemental information can be found online at https://doi.org/10.1016/j.checat.2022.03.016.

ACKNOWLEDGMENTS

This work was supported by the Natural Gas Innovation Fund, the Natural Sciences and Engineering Research Council of Canada (NSERC), the Natural Resources Canada Clean Growth Program, and the Ontario Research Fund – Research Excellence program. S.-F.H. acknowledges support from the Yushan Young Scholar Program, Ministry of Education, Taiwan.

AUTHOR CONTRIBUTIONS

E.H.S. supervised the project. A.S.R. conceived the idea and designed and carried out the experiments. J.W. and K.B. carried out the XPS. S.-F.H., F.-Y.W., and J.A. conducted and analyzed XAS experiments. J.E.H. contributed to the characterization of the materials. X.W., J.W., and C.-T.D. contributed to the discussion and results. All authors discussed the results and assisted during manuscript preparation.

DECLARATION OF INTERESTS

The authors declare no competing interests.

Received: December 5, 2021
Revised: March 9, 2022
Accepted: March 21, 2022
Published: April 12, 2022

REFERENCES

1. Vogt, C., Monai, M., Kramer, G.J., and Weckhuysen, B.M. (2019). The renaissance of the Sabatier reaction and its applications on Earth and in space. Nat. Catal. *2*, 188–197.

2. Jin, S., Hao, Z., Zhang, K., Yan, Z., and Chen, J. (2021). Advances and challenges for the electrochemical reduction of CO_2 to CO: from fundamentals to industrialization. Angew. Chem. Int. Ed. *60*, 20627–20648.

3. Zhang, L., Li, X.-X., Lang, Z.-L., Liu, Y., Liu, J., Yuan, L., Lu, W.-Y., Xia, Y.-S., Dong, L.-Z., Yuan, D.-Q., et al. (2021). Enhanced cuprophilic interactions in crystalline catalysts facilitate the highly selective electroreduction of CO_2 to CH_4. J. Am. Chem. Soc. *143*, 3808–3816.

4. Wang, R., Jiang, R., Dong, C., Tong, T., Li, Z., Liu, H., and Du, X.-W. (2021). Engineering a Cu/ZnO_x interface for high methane selectivity in CO_2 electrochemical reduction. Ind. Eng. Chem. Res. *60*, 273–280.

5. Li, Y., Xu, A., Lum, Y., Wang, X., Hung, S.-F., Chen, B., Wang, Z., Xu, Y., Li, F., Abed, J., et al. (2020). Promoting CO_2 methanation via ligand-stabilized metal oxide clusters as hydrogen-donating motifs. Nat. Commun. *11*, 6190.

6. Wang, X., Ou, P., Wicks, J., Xie, Y., Wang, Y., Li, J., Tam, J., Ren, D., Howe, J.Y., Wang, Z., et al. (2021). Gold-in-copper at low *CO coverage enables efficient electromethanation of CO_2. Nat. Commun. *12*, 3387.

7. Wang, X., Xu, A., Li, F., Hung, S.-F., Nam, D.-H., Gabardo, C.M., Wang, Z., Xu, Y., Ozden, A., Rasouli, A.S., et al. (2020). Efficient methane electrosynthesis enabled by tuning local CO_2 availability. J. Am. Chem. Soc. *142*, 3525–3531.

8. Xu, Y., Li, F., Xu, A., Edwards, J.P., Hung, S.-F., Gabardo, C.M., O'Brien, C.P., Liu, S., Wang, X., Li, Y., et al. (2021). Low coordination number copper catalysts for electrochemical CO_2 methanation in a membrane electrode assembly. Nat. Commun. *12*, 2932.

9. Yadav, R.M., Li, Z., Zhang, T., Sahin, O., Roy, S., Gao, G., Guo, H., Vajtai, R., Wang, L., Ajayan, P.M., et al. (2022). Amine-functionalized carbon nanodot electrocatalysts converting carbon dioxide to methane. Adv. Mater. *34*, 2105690.

10. Wang, Y., Liu, J., Wang, Y., Al-Enizi, A.M., and Zheng, G. (2017). Tuning of CO_2 reduction selectivity on metal electrocatalysts. Small *13*, 1701809.

11. Hori, Y., Kikuchi, K., Murata, A., and Suzuki, S. (1986). Production of methane and ethylene in electrochemical reduction of carbon dioxide at copper electrode in aqueous hydrogencarbonate solution. Chem. Lett. *15*, 897–898.

12. Sarfraz, S., Garcia-Esparza, A.T., Jedidi, A., Cavallo, L., and Takanabe, K. (2016). Cu–Sn bimetallic catalyst for selective aqueous electroreduction of CO_2 to CO. ACS Catal. *6*, 2842–2851.

13. Li, Y.C., Wang, Z., Yuan, T., Nam, D.-H., Luo, M., Wicks, J., Chen, B., Li, J., Li, F., de Arquer, F.P.G., et al. (2019). Binding site diversity promotes CO_2 electroreduction to ethanol. J. Am. Chem. Soc. *141*, 8584–8591.

14. Hoang, T.T.H., Verma, S., Ma, S., Fister, T.T., Timoshenko, J., Frenkel, A.I., Kenis, P.J.A., and Gewirth, A.A. (2018). Nanoporous copper–silver alloys by additive-controlled electrodeposition for the selective electroreduction of CO_2 to ethylene and ethanol. J. Am. Chem. Soc. *140*, 5791–5797.

15. Merino-Garcia, I., Albo, J., Solla-Gullón, J., Montiel, V., and Irabien, A. (2019). Cu oxide/ZnO-based surfaces for a selective ethylene production from gas-phase CO_2 electroconversion. J. CO2 Util. *31*, 135–142.

16. Huang, J., Mensi, M., Oveisi, E., Mantella, V., and Buonsanti, R. (2019). Structural sensitivities in bimetallic catalysts for electrochemical CO_2 reduction revealed by Ag–Cu nanodimers. J. Am. Chem. Soc. *141*, 2490–2499.

17. Gao, J., Zhang, H., Guo, X., Luo, J., Zakeeruddin, S.M., Ren, D., and Grätzel, M. (2019). Selective C–C coupling in carbon dioxide electroreduction via efficient spillover of intermediates as supported by operando Raman spectroscopy. J. Am. Chem. Soc. *141*, 18704–18714.

18. Nazir, R., Kumar, A., Saleh Saad, M.A., and Ashok, A. (2020). Synthesis of hydroxide nanoparticles of Co/Cu on carbon nitride surface via galvanic exchange method for electrocatalytic CO_2 reduction into formate. Colloids Surf. A Physicochem. Eng. Asp. *598*, 124835.

19. Zhi, X., Jiao, Y., Zheng, Y., Vasileff, A., and Qiao, S.-Z. (2020). Selectivity roadmap for electrochemical CO_2 reduction on copper-based alloy catalysts. Nano Energy *71*, 104601.

20. Zhong, M., Tran, K., Min, Y., Wang, C., Wang, Z., Dinh, C.-T., De Luna, P., Yu, Z., Rasouli, A.S., Brodersen, P., et al. (2020). Accelerated discovery of CO_2 electrocatalysts using active machine learning. Nature *581*, 178–183.

21. Gao, J., Ren, D., Guo, X., Zakeeruddin, S.M., and Grätzel, M. (2019). Sequential catalysis enables enhanced C–C coupling towards multi-carbon alkenes and alcohols in carbon dioxide reduction: a study on bifunctional

Cu/Au electrocatalysts. Faraday Discuss *215*, 282–296.

22. Dinh, C.-T., Burdyny, T., Kibria, M.G., Seifitokaldani, A., Gabardo, C.M., de Arquer, F.P.G., Kiani, A., Edwards, J.P., Luna, P.D., Bushuyev, O.S., et al. (2018). CO_2 electroreduction to ethylene via hydroxide-mediated copper catalysis at an abrupt interface. Science *360*, 783–787.

23. Liu, X., Schlexer, P., Xiao, J., Ji, Y., Wang, L., Sandberg, R.B., Tang, M., Brown, K.S., Peng, H., Ringe, S., et al. (2019). pH effects on the electrochemical reduction of CO_2 towards C_2 products on stepped copper. Nat. Commun. *10*, 32.

24. Cheng, M.-J., Clark, E.L., Pham, H.H., Bell, A.T., and Head-Gordon, M. (2016). Quantum mechanical screening of single-atom bimetallic alloys for the selective reduction of CO_2 to C_1 hydrocarbons. ACS Catal. *6*, 7769–7777.

25. Montoya, J.H., Shi, C., Chan, K., and Nørskov, J.K. (2015). Theoretical insights into a CO dimerization mechanism in CO_2 electroreduction. J. Phys. Chem. Lett. *6*, 2032–2037.

26. Valenti, M., Prasad, N.P., Kas, R., Bohra, D., Ma, M., Balasubramanian, V., Chu, L., Gimenez, S., Bisquert, J., Dam, B., et al. (2019). Suppressing H_2 evolution and promoting selective CO_2 electroreduction to CO at low overpotentials by alloying Au with Pd. ACS Catal. *9*, 3527–3536.

27. Ooka, H., Figueiredo, M.C., and Koper, M.T.M. (2017). Competition between hydrogen evolution and carbon dioxide reduction on copper electrodes in mildly acidic media. Langmuir *33*, 9307–9313.

28. Hori, Y., Wakebe, H., Tsukamoto, T., and Koga, O. (1994). Electrocatalytic process of CO selectivity in electrochemical reduction of CO_2 at metal electrodes in aqueous media. Electrochim. Acta *39*, 1833–1839.

29. Yan, C., Lin, L., Gao, D., Wang, G., and Bao, X. (2018). Selective CO_2 electroreduction over an oxide-derived gallium catalyst. J. Mater. Chem. A *6*, 19743–19749.

30. Tran, K., and Ulissi, Z.W. (2018). Active learning across intermetallics to guide discovery of electrocatalysts for CO_2 reduction and H_2 evolution. Nat. Catal. *1*, 696–703.

31. Verma, S., Hamasaki, Y., Kim, C., Huang, W., Lu, S., Jhong, H.-R.M., Gewirth, A.A., Fujigaya, T., Nakashima, N., and Kenis, P.J.A. (2018). Insights into the low overpotential electroreduction of CO_2 to CO on a supported gold catalyst in an alkaline flow electrolyzer. ACS Energy Lett. *3*, 193–198.

32. Luo, W., Zhang, J., Li, M., and Züttel, A. (2019). Boosting CO production in electrocatalytic CO_2 reduction on highly porous Zn catalysts. ACS Catal. *9*, 3783–3791.

33. Zhan, C., Dattila, F., Rettenmaier, C., Bergmann, A., Kühl, S., García-Muelas, R., López, N., and Cuenya, B.R. (2021). Revealing the CO coverage-driven C–C coupling mechanism for electrochemical CO_2 reduction on Cu_2O nanocubes via operando Raman spectroscopy. ACS Catal. *11*, 7694–7701.

34. Zhang, H., Chang, X., Chen, J.G., Goddard, W.A., Xu, B., Cheng, M.-J., and Lu, Q. (2019). Computational and experimental demonstrations of one-pot tandem catalysis for electrochemical carbon dioxide reduction to methane. Nat. Commun. *10*, 3340.

35. Li, J., Wang, Z., McCallum, C., Xu, Y., Li, F., Wang, Y., Gabardo, C.M., Dinh, C.-T., Zhuang, T.-T., Wang, L., et al. (2019). Constraining CO coverage on copper promotes high-efficiency ethylene electroproduction. Nat. Catal. *2*, 1124–1131.

36. Ren, D., Ang, B.S.-H., and Yeo, B.S. (2016). Tuning the selectivity of carbon dioxide electroreduction toward ethanol on oxide-derived Cu_xZn catalysts. ACS Catal. *6*, 8239–8247.

37. Zhang, Y.-J., Sethuraman, V., Michalsky, R., and Peterson, A.A. (2014). Competition between CO_2 reduction and H_2 evolution on transition-metal electrocatalysts. ACS Catal. *4*, 3742–3748.

38. da Silva, A.G.M., Rodrigues, T.S., Haigh, S.J., and Camargo, P.H.C. (2017). Galvanic replacement reaction: recent developments for engineering metal nanostructures towards catalytic applications. Chem. Commun. *53*, 7135–7148.

39. Papaderakis, A., Mintsouli, I., Georgieva, J., and Sotiropoulos, S. (2017). Electrocatalysts prepared by galvanic replacement. Catalysts *7*, 80.

40. Papadimitriou, S., Tegou, A., Pavlidou, E., Armyanov, S., Valova, E., Kokkinidis, G., and Sotiropoulos, S. (2008). Preparation and characterisation of platinum- and gold-coated copper, iron, cobalt and nickel deposits on glassy carbon substrates. Electrochim. Acta *53*, 6559–6567.

41. Wang, X., Ou, P., Ozden, A., Hung, S.-F., Tam, J., Gabardo, C.M., Howe, J.Y., Sisler, J., Bertens, K., García de Arquer, F.P., et al. (2022). Efficient electrosynthesis of n-propanol from carbon monoxide using a Ag–Ru–Cu catalyst. Nat. Energy *7*, 170–176.

42. Conway, B.E., and Jerkiewicz, G. (2000). Relation of energies and coverages of underpotential and overpotential deposited H at Pt and other metals to the 'volcano curve' for cathodic H_2 evolution kinetics. Electrochim. Acta *45*, 4075–4083.

43. Gabardo, C.M., O'Brien, C.P., Edwards, J.P., McCallum, C., Xu, Y., Dinh, C.-T., Li, J., Sargent, E.H., and Sinton, D. (2019). Continuous carbon dioxide electroreduction to concentrated multi-carbon products using a membrane electrode assembly. Joule *3*, 2777–2791.

44. Jeanty, P., Scherer, C., Magori, E., Wiesner-Fleischer, K., Hinrichsen, O., and Fleischer, M. (2018). Upscaling and continuous operation of electrochemical CO_2 to CO conversion in aqueous solutions on silver gas diffusion electrodes. J. CO2 Util. *24*, 454–462.

45. Sedighian Rasouli, A., Wang, X., Wicks, J., Lee, G., Peng, T., Li, F., McCallum, C., Dinh, C.-T., Ip, A.H., Sinton, D., et al. (2020). CO_2 electroreduction to methane at production rates exceeding 100 mA/cm^2. ACS Sustain. Chem. Eng. *8*, 14668–14673.

46. Rabinowitz, J.A., and Kanan, M.W. (2020). The future of low-temperature carbon dioxide electrolysis depends on solving one basic problem. Nat. Commun. *11*, 5231.